Published in final edited form as:
Biomaterials. 2009 April ; 30(10): 1928–1936. doi:10.1016/j.biomaterials.2008.12.038.

Influence of anchoring ligands and particle size on the colloidal stability and *in vivo* biodistribution of polyethylene glycol-coated gold nanoparticles in tumor-xenografted mice

Guodong Zhang[a], **Zhi Yang**[a], **Wei Lu**[a], **Rui Zhang**[a], **Qian Huang**[a], **Mei Tian**[a], **Li Li**[b], **Dong Liang**[c], and **Chun Li**[a,*]

[a]Department of Experimental Diagnostic Imaging, The University of Texas M. D. Anderson Cancer Center, Houston, TX 77030, USA

[b]The Brown Institute of Molecular Medicine, The University of Texas Health Science Center at Houston, Houston, TX 77030, USA

[c]Department of Pharmaceutical Sciences, Texas Southern University, Houston, TX 77004, USA

Abstract

Polyethylene glycol (PEG)-coated (pegylated) gold nanoparticles (AuNPs) have been proposed as drug carriers and diagnostic contrast agents. However, the impact of particle characteristics on the biodistribution and pharmacokinetics of pegylated AuNPs is not clear. We investigated the effects of PEG molecular weight, type of anchoring ligand, and particle size on the assembly properties and colloidal stability of PEG-coated AuNPs. The pharmacokinetics and biodistribution of the most stable PEG-coated AuNPs in nude mice bearing subcutaneous A431 squamous tumors were further studied using ^{111}In-labeled AuNPs. AuNPs coated with thioctic acid (TA)-anchored PEG exhibited higher colloidal stability in phosphate-buffered saline in the presence of dithiothreitol than did AuNPs coated with monothiol-anchored PEG. AuNPs coated with high-molecular-weight (5000 Da) PEG were more stable than AuNPs coated with low-molecular-weight (2000 Da) PEG. Of the 20-nm, 40-nm, and 80-nm AuNPs coated with TA-terminated PEG_{5000}, the 20-nm AuNPs exhibited the lowest uptake by reticuloendothelial cells and the slowest clearance from the body. Moreover, the 20-nm AuNPs coated with TA-terminated PEG_{5000} showed significantly higher tumor uptake and extravasation from the tumor blood vessels than did the 40- and 80-nm AuNPs. Thus, 20-nm AuNPs coated with TA-terminated PEG_{5000} are promising potential drug delivery vehicles and diagnostic imaging agents.

Keywords

Gold nanoparticle; Polyethylene glycol; Thioctic acid; Biodistribution; Pharmacokinetics

1. Introduction

Gold nanoparticles (AuNPs) ranging from 2 to 200 nm in diameter have excellent biocompatibility, an amendable method for surface modification, and attractive

*Corresponding author. Department of Experimental Diagnostic Imaging-Box 59, The University of Texas M. D. Anderson Cancer Center, 1515 Holcombe Boulevard, Houston, TX 77030, USA. Tel.: +1 713 792 5182; fax: +1 713 794 5456. cli@di.mdacc.tmc.edu (C. Li).
Z. Yang is on leave from the Department of Nuclear Medicine, Peking University School of Oncology and Beijing Cancer Hospital, Beijing, China 100036

physicochemical properties. These nanoparticles have been proposed in diverse biomedical applications including advanced drug delivery, photothermal ablation therapy, and molecular diagnostics [1-3]. However, plasma proteins in blood adsorb onto the surface of bare AuNPs, which produces large aggregates [4] that may result in altered pharmacokinetics and biodistribution of AuNPs [5]. Polyethylene glycol (PEG) is found to minimize nonspecific adsorption of proteins onto nanoparticles and to reduce their uptake by the liver [5]. For example, 30-nm PEG-coated AuNPs have been successfully used to deliver tumor necrosis factor to solid tumors [6]; and PEG-coated AuNPs have also been reported to be promising computed tomography (CT) contrast agents for blood pool imaging because they exhibit a longer blood circulation time and 5.7 times higher attenuation than the iodine-based CT contrast agents that are currently used [7,8]. Qian et al. [9] described the use of pegylated AuNPs for *in vivo* tumor targeting and molecular imaging based on their surface-enhanced Raman scattering effect. In addition, AuNPs have been shown to be highly sensitive colloidal biosensors on the basis of their aggregation behavior [10].

Despite the potential benefits of AuNPs in biomedical applications, little is known about the fate of AuNPs *in vivo*, particularly with regard to the effects the particles' characteristics have on their pharmacokinetics and biodistribution.

Particle size is one such characteristic. After intravenous injection into rats, spherical AuNPs ranging from 10 to 250 nm in diameter have been shown to be taken up primarily by the liver and spleen, with the 10-nm nanoparticles more broadly distributed in various organs [11]. Recent work indicates that gold nanospheres, nanoshells, and nanorods coated with PEG exhibit prolonged circulation time *in vivo* upon systemic injection [6,12,13]. However, to the best of our knowledge, the effects of particle size on the biodistribution and pharmacokinetics pegylated AuNPs have not been reported.

The method of attaching PEG to AuNPs is another factor that may affect the colloidal stability and thus pharmacokinetics and biodistribution of pegylated AuNPs. One method of covalently attaching PEG to AuNPs is through the use of a thiol-terminated PEG (PEG-SH). Foos et al. [14] used this approach to synthesize water-soluble AuNPs. Tshikhudo et al. [15] synthesized water-soluble AuNPs by coating particles with PEG chains anchored through alkanethiol groups. Indeed, pegylated AuNPs used in previous *in vivo* studies were all prepared using PEG-SH [6,12,13]. Another method of attaching PEG to the surfaces of AuNPs is to use PEG that contains multiple thiol groups that act as anchoring ligands. Studies have shown that AuNPs coated with oligonucleotides modified with multiple thiol groups have significantly improved colloidal stability compared to AuNPs coated with monothiol-terminated oligonucleotides [16,17]. AuNPs can also be coated with PEG attached to thioctic acid (TA), also known as alpha-lipoic acid, a naturally occurring compound. TA is particularly well suited for gold surface modification because as a cyclic disulfide-containing compound, it gives added stability by providing two gold-sulfur bonds per molecule in surface-functionalized gold [18].

The aims of the current study were: 1) to evaluate the effects of the conjugation chemistry and molecular weight of PEG on the colloidal stability of pegylated AuNPs and 2) to determine the influence of particle size (20–80 nm) on the *in vivo* pharmacokinetics and biodistribution of the most stable pegylated AuNPs in tumor-bearing mice. To facilitate the *in vivo* study, a gamma emitter, indium-111 (^{111}In, half-life [$t_{1/2}$] = 2.7 days), was introduced to AuNPs via a radiometal chelator, diethylenetriaminepentaacetic acid (DTPA). Previous biodistribution studies of AuNPs used inductively coupled plasma-mass spectrometry [6,13] or neutron activation analysis [12] to quantitatively analyze gold concentration in excised tissues. These methods involve a series of tedious operations and do not allow repetitive assessment of tissue distribution in live animals. In comparison, the radiotracer method is highly sensitive, easily

quantifiable, and allows repetitive, noninvasive imaging. The radiotracer method has become a powerful tool for evaluating the biodistribution of various nanoparticles, including polymeric micelles [19,20], gelatin nanoparticles [21], and carbon nanotubes [22].

2. Materials and methods

2.1. Materials

AuNP colloids with average diameters of 20, 40, and 80 nm were purchased from Ted Pella, Inc. (Redding, CA). 1-Ethyl-3-(3-dimethylaminopropyl) carbodiimide hydrochloride (EDC HCl) and 1,3-diisopropylcarbodiimide were obtained from Pierce (Rockford, IL). O-(2-aminoethyl)-O′-methylpolyethylene glycol with molecular weights of 2000 (MeO-PEG_{2000}-NH_2) and 5000 (MeO-PEG_{5000}-NH_2) were obtained from Fluka (Buchs, Switzerland). O-(2-thioethyl)-O′-methylpolyethylene glycol with a molecular weight of 5000 (MeO-PEG_{5000}-SH) was purchased from Nektar (Huntsville, AL). Diisopropylethylamine, *N*-hydroxysuccinimide, TA, and all solvents were obtained from Acros (Morris Plains, NJ). Spectra/Por dialysis membrane (molecular weight cutoff = 1000) was purchased from Spectrum Laboratories (Rancho Dominguez, CA). *p*-Aminobenzyl-diethylenetriaminepenta-*tert*-butyl ester was synthesized as previously described [23]. Rat anti-mouse platelet-endothelial cell adhesion molecule-1 (CD31) monoclonal antibody and rabbit monoclonal antibody against epidermal growth factor receptor (EGFR) were purchased from Millipore (Temecula, CA). Alexa fluor 594-conjugated goat anti-rat immunoglobulin G (IgG) and Alexa fluor 488-conjugated goat anti-rabbit IgG were obtained from Molecular Probes (Eugene, OR). The radioactive tracer $^{111}InCl_3$ was obtained from Iso-Tex Diagnostics (Houston, TX).

2.2. Characterization of physicochemical properties

^{1}H- and ^{13}C-nuclear magnetic resonance (NMR) spectra were recorded on a Bruker Avance 300 spectrometer (Billerica, MA); tetramethylsilane was used as an internal standard. Matrix-assisted laser desorption/ionization time-of-flight (MALDI-TOF) spectra were measured on a Voyager-DE-STR MALDI-TOF mass spectrometer (Applied Biosystems, Framingham, MA) equipped with a nitrogen laser emitting a 337-nm wavelength. Spectra were acquired in the linear-positive mode with delayed extraction. Samples were prepared by mixing 10 μl of the sample solution (1 mg/ml) with 10 μl of 2,5-dihydroxybenzoic acid in tetrahydrofuran (10 mg/ml). The number-average molecular weight (Mn) and weight-average molecular weight (Mw) were calculated from the MALDI-TOF spectra using Data Explorer software (Applied Biosystems, Framingham, MA). Electrospray ionization mass spectrometry (ESI-MS) data were obtained on an Agilent 1100 Series LC/MSD Trap high-performance ion-trap mass spectrometer visible light instrument (Santa Clara, CA). Ultraviolet-visible (UV-Vis) spectra of the AuNPs were recorded on a Beckman Coulter DU 800 UV-Vis spectrophotometer with a quartz cuvette with a 10-mm optical path length (Fullerton, CA).

Particle size was measured using dynamic light scattering at a 90° scatter angle on a ZetaPLUS particle electrophoresis system (Brookhaven Instruments Corp., Holtsville, NY). Correlation data were analyzed using a BI-9000AT Digital Autocorrelator (Brookhaven), and a nonnegatively constrained least squares (CONTIN) approximation was used to calculate the particle size distribution. Zeta (ζ) potential for the AuNPs was determined with the ZetaPLUS system. Data were acquired in the phase analysis light scattering mode at 25°C, and sample solutions were prepared by diluting AuNPs into 10 mM phosphate-buffered saline (PBS) solution (pH 7.0). Results were given as the mean value of 10 measurements.

2.3. Synthesis of thioctic acid N-hydroxysuccinimide (TA-NHS)

TA-NHS was synthesized as previously described. [17]. Briefly, to a solution of EDC HCl (1.840 g, 9.6 mmol, 1.2 Eq) and diisopropylethylamine (1.7 ml, 9.6 mmol, 1.2 Eq) in 20 ml

anhydrous dichloromethane (DCM), was added *N*-hydroxysuccinimide (1.290 g, 11.2 mmol, 1.4 eq), and the mixture was stirred in an ice bath. TA (1.643 g, 8.0 mmol, 1.0 Eq) solution in anhydrous DCM (10 ml) was subsequently added over 5 min, and the reaction mixture was stirred at room temperature overnight. The reaction mixture was washed with aqueous HCl solution (5% vol/vol) twice and then washed with deionized water. The organic layer was dried over Na_2SO_4. Solvents were removed under vacuum. The residue was purified by flash column chromatography to yield 2.02 g of TA-NHS (83%) as a yellow solid: ^{1}H NMR ($CDCl_3$), δ (ppm): 3.56 (sextet, 1H, J = 4.0 Hz, S-S-**CH_2**-), 3.16 (sextet, 1H, J = 4.0 Hz, S-S-**CH_2**-), 3.10 (sextet, 1H, J = 4.0 Hz, S-S-**CH**-), 2.82 (d, 4H, J = 1.0 Hz, -CO**CH_2CH_2**CO-), 2.61 (t, 2H, J = 2.0 Hz,-**CH_2**CO-), 2.44 (sextet, 1H, J = 6.0 Hz, S-CH_2-**CH_2**-), 1.90 (sextet, 1H, J = 6.0 Hz, S-CH_2-**CH_2**-), 1.72-1.78 (m, 2H, -**CH_2**-CH_2-CO-), 1.67-1.70 (m, 2H, -CH-**CH_2**-CH_2-), 1.52-1.56 (m, 2H, -CH-CH_2-**CH_2**-). ^{13}C NMR ($CDCl_3$): δ169.34, 168.62, 56.29, 40.36, 38.72, 34.62, 30.98, 28.53, 25.79, 24.56. ESI-MS: calcd. for $C_{12}H_{18}NO_4S_2$ $(M+H)^+$: 304.0677; found: 304.0612.

2.4. Synthesis of MeO-PEG_{2000}-NH-Thioctic Acid (PEG_{2000}-TA)

PEG-TA was synthesized according to Dixit et al. [18] with some modifications. Instead of refluxing the reaction mixture containing PEG-NH_2 and TA-NHS in DCM, the reaction was allowed to proceed at room temperature. Briefly, MeO-PEG_{2000}-NH_2 (0.5 g, 0.25 mmol) and TA-NHS (143 mg, 0.5 mmol) were dissolved in 10 ml anhydrous DCM, and dry triethylamine (0.5 ml, 4.0 mmol) was then added dropwise. The reaction solution was stirred at room temperature overnight. The progress of the reaction was monitored using thin-layer chromatography (silica plate, 10% methanol in chloroform, iodine stain). After organic solvent was removed under vacuum, the crude product was dissolved in methanol and dialyzed against methanol until all starting materials disappeared on the thin-layer chromatography plate. The solution was then dialyzed against deionized water. The aqueous solution of purified product was lyophilized to yield PEG_{2000}-TA (0.40 g, 86%). ^{1}H NMR ($CDCl_3$), δ (ppm): 3.89 (t, 2H, J = 2.4 Hz, -NH**CH_2**CH_2O-), 3.74-3.55 (m, 200H, -OC**H_2CH_2O**-), 3.48-3.43 (m, 1H, TA), 3.20-3.11 (m, 3H, -O**CH_3**), 2.50-2.42 (m, 1H, TA), 2.20 (t, 2H, J = 2.0 Hz, TA), 1.95-1.89 (m, 1H, TA), 1.75-1.66 (m, 6H, TA), 1.52-1.47(m, 2H, TA). MALDI-TOF Mass: Mn: 2234.17, Mw/Mn: 1.02.

PEG_{5000}-TA was synthesized using identical procedures. Yield: 0.60 g (80%). ^{1}H NMR [$CDCl_3$], δ (ppm): 3.90 (t, 2H, J = 2.4 Hz, -NH**CH_2**CH_2O-), 3.74-3.55 (m, 500H, -OC**H_2CH_2O**-), 3.50-3.43 (m, 1H, TA), 3.20-3.11 (m, 3H, -O**CH_3**), 2.50-2.40 (m, 1H, TA), 2.22 (t, 2H, J = 2.0 Hz, TA), 1.95-1.89 (m, 1H, TA), 1.75-1.66 (m, 6H, TA), 1.50-1.47(m, 2H, TA). MALDI-TOF Mass: Mn: 5238.54, Mw/Mn: 1.01.

2.5. Synthesis of 4-aminobenzyl-diethylenetriaminepentaacetic acid thioctamide (DTPA-TA)

TA (260 mg, 1.26 mmol) and *p*-aminobenzyl-diethylenetriaminepenta-*tert*-butyl ester (983 mg, 1.26 mmol) were dissolved in 8 ml of anhydrous DCM. 1,3-Diisopropylcarbodiimide (159 mg, 1.26 mmol), 0.43 ml pyridine, and a catalytic amount of 4-dimethylaminopyridine were added to the reaction solution. The mixture was stirred at room temperature overnight. To stop the reaction, the DCM solution was washed twice with water. The organic phase was dried over anhydrous sodium sulfate. After removal of solvent under vacuum, the crude product was purified using silica chromatography (eluent, ethyl acetate/hexane; 3/1 vol/vol) to yield as yellow powder (1.12 g, 75%). The protecting groups were removed by treating DTPA(penta *tert*-butyl ester)-TA in 2 ml of DCM with 2 ml of trifluoroacetic acid at room temperature. The solvent and trifluoroacetic acid were evaporated under vacuum, and the residue was dissolved in methanol and then precipitated into cold ethyl ether to yield DTPA-TA as a yellow solid (0.68 g, 86%). ^{1}H NMR (D_2O, pD = 9.0), δ ppm: 7.36-7.21(AA′BB′-system, aromatic, 4H); 3.74-3.67 (m, 1H, TA), 3.37-3.02 (m, 13H, 6 × -CH_2- and -CH- of DTPA), 2.79-2.39 (m, 10H,

3 × -CH_2- of DTPA, TA), 2.31-2.10 (m, 1H, TA), 2.05-1.94(m, 1H, TA), 1.81-1.65 (m, 4H, TA), 1.53-1.45 (m, 2H, TA). ^{13}C NMR (DMSO-d_6): δ173.87, 172.30, 170.96, 167.77, 141.60, 137.76, 132.16, 129.29, 119.09, 118.42, 116.49, 116.03, 114.56, 113.13, 112.64, 110.86, 58.98, 56.08, 55.30, 53.83, 51.15, 48.68, 38.07, 34.14, 31.26, 30.73, 28.34, 27.01, 24.86, 23.88. ESI-MS: calcd. for $C_{29}H_{43}N_4O_{11}S_2$ $(M+H)^+$: 687.2370; found: 687.2340.

2.6. Preparation of PEG-coated AuNPs

Five milliliters of the aqueous solution of PEG-TA or PEG-SH (100 μg/ml) was added to 5 ml of AuNPs suspended in water (9.0×10^{10} AuNPs/ml), and the mixture was stirred overnight at room temperature. To remove the unreacted PEG precursor from the solution, AuNPs were centrifuged at 13,000 rpm for 10 min, the supernatant was decanted, and the particles were resuspended in PBS; this was done three times. PEG-coated AuNPs were suspended in 5 ml of PBS and stored at 4°C.

2.7. Preparation of PEG-coated, DTPA-conjugated AuNPs

A solution of DTPA-TA (100 μl, 10 μg/ml) was added to 10 ml of AuNPs suspended in 10 mM sodium dicarbonate (9.0×10^{10} nanoparticles/ml). The mixture was then sonicated (VWR Ultrasonic Model 250T, West Chester, PA) at room temperature for 30 min. Next, 10 ml of the aqueous solution of PEG-TA (100 μg/ml) was added and the reaction mixture was stirred overnight. The resulting nanoparticles were purified by centrifugation/washing as described in the preceding section, suspended in 0.2 ml of 0.1 M sodium acetate solution (pH 5.5), and stored at 4°C.

2.8. Stability of PEG–coated AuNPs

Dithiothreitol (DTT) was added to each preparation of PEG-coated AuNPs in PBS solution to a final concentration of 10 mM. The solution was degassed with inert Ar gas and incubated at 40°C. Aliquots of AuNP solution were removed, and their UV-Vis spectra were recorded at different times after addition of DTT. Stability was evaluated by measuring the increment of absorbance at 650 nm that resulted from AuNP aggregation.

To simulate physiological conditions, we incubated PEG-coated AuNPs in PBS containing 10% fetal bovine serum (FBS) at 37°C. Colloidal stability was monitored by measuring changes in particle size using dynamic light scattering.

2.9. ^{111}In labeling of PEG-coated, DTPA-conjugated AuNPs

Aliquots of PEG-coated, DTPA-conjugated AuNPs (4.5×10^{12} nanoparticles/ml, 0.2 ml) in 0.1 M sodium acetate solution (pH 5.5) were mixed with an aqueous solution of $^{111}InCl_3$ (520 μCi) at room temperature for 30 min. The labeled nanoparticles were analyzed using instant thin-layer chromatography. The paper strips were developed with PBS (pH 7.4) containing 4 mM ethylenediaminetetraacetic acid and quantified using a Bioscan IAR-2000 thin-layer chromatography imaging scanner (Washington, DC). Free $^{111}In^{3+}$ moved to the solvent front (relative front = 0.9–1.0), and the nanoparticles remained at the original spot (relative front = 0.0). The labeling efficiency for 20-nm and 40-nm AuNPs was > 95%, and the labeling efficiency for 80-nm AuNPs was 93%.

2.10. Pharmacokinetics

All animal studies were carried out in the Small Animal Imaging Facility at The University of Texas M. D. Anderson Cancer Center in accordance with institutional guidelines. Eight healthy female BALB/c mice (22–25 g; Charles River Laboratories, Wilmington, MA) were each injected intravenously with a dose of 1.0×10^{11} AuNPs (60 μCi). At predetermined intervals, blood samples (10 μl) were taken from the tail vein, and the radioactivity of each sample was

measured with a Cobra Autogamma counter (Packard, Downers Grove, IL). The blood pharmacokinetic parameters of the radiotracer were analyzed with a two-compartmental model using WinNonlin 5.0.1 software (Pharsight Corporation, Palo Alto, CA). Animals were euthanized by CO_2 exposure at the end of the study. Values are expressed as means ± standard deviations calculated for 8 mice from each group.

2.11. Biodistribution and gamma imaging in tumor-bearing mice

The human squamous carcinoma A431 cell line was obtained from American Type Cell Culture (Rockville, MD). Cells were maintained at 37°C in a humidified atmosphere containing 5% CO_2 in Dulbecco's modified Eagle's medium and Ham's nutrient mixture F-12 containing 10% FBS (GIBCO, Grand Island, NY).

A431 cells (1×10^6 cells suspended in PBS) were inoculated subcutaneously into the right forelegs of nude mice (20–25 g; Harlan Sprague Dawley, Inc., Indianapolis, IN). When the tumors had grown to 6–8 mm in average diameter, the mice were randomly allocated into 3 groups, with each group consisting of 3 mice. Mice in each group were injected intravenously with ^{111}In-labeled pegylated AuNPs (1.7×10^{10} nanoparticles/mouse, 10 μCi/mouse) and killed 48 h after injection. Blood, heart, liver, spleen, kidney, lung, stomach, intestine, muscle, bone, and tumor tissues were removed and weighed. Radioactivity was measured with a gamma counter. Uptake of contrast agent in various tissues was calculated as the percentage of the injected dose per gram of tissue (%ID/g).

For gamma imaging, mice bearing subcutaneous A431 tumors were injected intravenously with ^{111}In-labeled pegylated 20-nm or 80-nm AuNPs at a dose of 150 μCi/mouse (2.6×10^{11} nanoparticles/mouse). Mice were placed in the prone position. Anesthesia was initiated prior to imaging with 2% isoflurane gas (Iso-Thesia, Rockville, NY) in oxygen and maintained during imaging with 0.5–1.5% isoflurane in oxygen. Gamma images were acquired using an MCam camera equipped with a medium-energy collimator and ICON software (Siemens, Hoffman Estates, IL) using the following parameters: matrix, 512 × 512 pixels; zoom, 3.20×; energy peak, 247 keV (15%) and 172 keV (15%); total counts, 800 K.

2.12. Intratumoral Distribution

The resected A431 tumors from mice injected with 20-nm AuNPs at the end of the last imaging session (48 h after injection) were dissected for cryosection (5 μm per slice). The tissue sections were fixed with cold acetone at −20°C for 20 min. After washing with PBS, the sections were blocked by 10% goat serum for 30 min at 37°C and then stained with rat anti-mouse CD31 monoclonal antibody (1:100) and rabbit anti-mouse EGFR antibody (1:50) at 4°C overnight. After staining, the sections were washed with PBS. Alexa fluor 594-conjugated goat anti-rat IgG and Alexa fluor 488-conjugated goat anti-rabbit IgG (each at a 1:500 dilution) were then added, and the slices were incubated for 1 h at room temperature. After washing with PBS, the samples were mounted on slides for fluorescent microscope examination. Texas red and fluorescein isothiocyanate filter sets were used to visualize CD31 and EGFR expression, respectively, and a dark field condenser was used to visualize AuNPs. The tissue slices were examined under a Zeiss Axio Observer.Z1 fluorescence microscope (Carl Zeiss MicroImaging GmbH, Göttingen, Germany). A Hamamatsu chilled charge-coupled-device camera (Hamamatsu Photonics K. K., Hamamatsu, Japan) was used to obtain photomicrographs of the tissue samples.

2.13. Statistical analysis

Statistical analysis of pharmacokinetic parameters was conducted using analysis of variance with Tukey's post hoc test (SYSTAT for Windows 11, SYSTAT Software, Inc., San Jose, CA).

Differences in biodistribution data were analyzed using a two-tailed unpaired Student's *t*-test. *P* values < 0.05 were considered statistically significant.

3. Results and discussion

3.1. Synthesis of PEG-TA and DTPA-TA

The reaction schemes for the synthesis of PEG_{2000}-TA and DTPA-TA and their introduction to AuNPs are shown in Figure 1. PEG-TA was obtained by mixing solutions of PEG-NH_2 and TA-NHS in DCM at room temperature. Thin-layer chromatography analysis confirmed that the reaction was complete in 12 h. For purification, dialysis against methanol effectively removed the small-molecular-weight contaminants. ^{1}H NMR spectra revealed the characteristic peaks of TA in PEG_{2000}-TA. The integral ratio of -O$\mathbf{CH_2CH_2}$O- in PEG moiety (3.55–3.74 ppm) vs. -CH-CH_2-$\mathbf{CH_2}$- in TA moiety (1.47–1.52 ppm) was consistent with the average degree of polymerization of 44 for PEG. The structure of PEG_{2000}-TA was further confirmed by MALDI-TOF mass spectroscopy, which showed Mn ranging from 1871 to 2665, which corresponded to PEG with degrees of polymerization that ranged from 36 to 54 terminated with a TA (with one Na^+ counter ion) and a methoxy group (Fig. 2). The structure of PEG_{5000}-TA was similarly confirmed.

DTPA-TA was synthesized via a diisopropylcarbodiimide-mediated coupling reaction between TA and aminobenzyl DTPA(penta-*t*-butyl ester) (Fig. 1). The crude product was purified by silica gel chromatography followed by quantitative removal of *t*-butyl-protecting groups with trifluoroacetic acid. The structure of DTPA-TA was confirmed by ^{1}H-NMR and ESI-MS.

3.2. PEG-coated AuNPS

PEG-TA was attached to AuNPs by mixing PEG-TA with aqueous solution of AuNPs under the protection of inert Ar gas. To determine the effect of anchoring chemistry on the colloidal stability of AuNPs, AuNPs were also coated with. ^{1}H NMR indicated that PEG-TA and PEG-SH molecules were conjugated to AuNPs (data not shown).

The physicochemical properties of AuNPs coated with PEG-TA and PEG-SH are summarized in Table 1. Owing to their citric acid coating, all AuNPs were highly negatively charged before pegylation, with ζ potentials ranging from −34 to −41 mV. Introducing a layer of PEG to the AuNPs masked the negative charge and resulted in almost neutral AuNPs (ζ potential < −10 mV). On the basis of dynamic light scattering measurements, the thicknesses of the PEG_{5000}-TA coatings on the 20-nm, 40-nm, and 80-nm AuNPs were estimated to be 12.7, 9.8, and 4.7 nm, respectively. PEG layer thickness appeared to depend on the curvature of the AuNPs: the smaller the AuNPs, the thicker the PEG layer. A similar trend was observed when AuNPs were coated with lower-molecular-weight PEG_{2000}-TA and with PEG_{5000}-SH. This phenomenon has been described by Hurst et al. [24] in terms of coverage density, i.e., the coverage density with DNA-PEG-SH on AuNPs decreases as particle size increases. Theoretically, the end-to-end distances of PEG_{5000} for zigzag, meander, and random coil models are 39.7, 20.4–22.7, and 4.9 nm, respectively [25]. Therefore, the PEG chains coating smaller 20-nm AuNPs adopted a more stretched meander conformation, whereas PEG chains on the larger 40- and 80-nm AuNPs adopted a random-coil conformation.

3.3. Colloidal stability of PEG-coated AuNPs

The colloidal stability of AuNPs coated with PEG-TA or PEG-SH was evaluated by assessing the formation of AuNP aggregates in the presence of 10 mM DTT at 40°C [16,17]. Detachment of PEG from AuNPs would cause the nanoparticles to aggregate, which could be monitored by measuring the disappearance of the characteristic plasmon absorption band at ~520 nm and

the appearance of a peak between 600 and 700 nm. Typical UV-Vis spectra of PEG_{5000}-TA-coated 40-nm AuNPs are shown in Figure 3A. Figure 3B shows the changes in signal intensity at the 650-nm peak versus incubation time in the presence of DTT. The time required for the peak at 650 nm to reach half of the maximum intensity, $t_{1/2}$, was used to measure the stability of the PEG-gold bond. The stability data thus obtained for pegylated AuNPs are summarized in Figure 3C. Of the pegylated AuNPs evaluated, 20-nm AuNPs coated with PEG_{5000}-TA were most stable. For 20- and 40-nm AuNPS, AuNPs coated with PEG-TA were more stable than AuNPs coated with PEG-SH of the same molecular weight. The following factors are possible mechanisms for improved stability for AuNPs coated with PEG-TA: 1) TA may provide a dense and ordered coating layer [26], and 2) Bonds formed between TA and gold are different from those formed between thiol and gold. For 80-nm AuNPs, a rapid reduction in absorbance at 560 nm was observed upon the addition of DTT regardless of whether TA or thiol was used to anchor PEG (data not shown). It was not clear why pegylation chemistry had a limited effect in stabilizing larger AuNPs in the presence of DTT. It is possible that in 80-nm AuNPS, the PEG coating layer was not as dense as that in the smaller AuNPs, which allowed DTT molecules to gain easy access to the Au-S bonds in PEG-TA coated surface.

To evaluate the stability of pegylated AuNPs under physiological conditions, AuNPs were incubated in PBS containing 10% FBS at 37°C. Changes in particle size were monitored using dynamic light scattering. Particle size variation as a function of incubation time for 20-nm AuNPs coated with PEG_{2000}-TA, PEG_{5000}-TA, or PEG_{2000}-SH is presented in Figure 4. The size of these particles remained unchanged for 48 h. In contrast, the size of uncoated AuNPs increased 2–5 times within 10 min of exposure to PBS containing FBS (Fig. 4); during this time, the AuNP solution also changed from its original pinkish color to a light blue color, indicating formation of particle aggregates. Pegylated 40-nm AuNPs displayed similar colloidal stability in the presence of serum proteins as that observed with pegylated 20-nm AuNPs. However, pegylated 80-nm AuNPs were less stable than smaller particles: precipitation of particle aggregates was observed over 24 h. These results indicate that the dense, thick PEG layer effectively insulated AuNPs from nonspecific binding to proteins and thus enhanced the colloidal stability of pegylated AuNPs.

3.4 Pharmacokinetics of PEG–coated AuNPs

Because AuNPs coated with PEG_{5000}-TA were the most stable AuNPs based on our *in vitro* findings, their *in vivo* pharmacokinetics and biodistribution were further evaluated. Radiometal chelator DTPA-TA and then PEG-TA were conjugated to the AuNPs. We expected that the PEG layer would mask the DTPA molecules, thus minimizing any potential effect of DTPA on the surface properties of pegylated AuNPs. Indeed, the surface characteristics of pegylated AuNPs containing immobilized DTPA were similar to those of pegylated AuNPs without DTPA. For example, the ζ potentials of pegylated 20-nm and 40-nm AuNPs containing DTPA were −7.5 mV and −6.9 mV, respectively. These values were similar to the ζ potentials of both pegylated 20-nm and 40-nm AuNPs without DTPA (both were -8.1 mV).

Figure 5 shows the mean blood activity-time profile of ^{111}In-labeled PEG_{5000}-TA-coated AuNPs. The 40- and 80-nm AuNPs were cleared rapidly from the blood, whereas the small 20-nm AuNPs had higher blood activity at all time points. For example, 8 h after drug administration, 20-nm AuNPs had a significant 1.4- to 10-fold higher blood activity than that of 40- and 80-nm AuNPs (55.2 ± 3.0% vs 39.1 ± 4.6% and 5.23 ± 2.8% of the injected dose per ml of blood, respectively). The pharmacokinetic parameters of AuNPs of different sizes coated with PEG_{5000}-TA after intravenous injection are summarized in Table 2. Compared to 40- and 80-nm AuNPs, 20-nm AuNPs exhibited a higher area-under-the-curve in blood, longer mean residence time (the average time that a drug molecule stays in the body), longer terminal elimination half-life ($t_{1/2\beta}$), and lower total body clearance rate. The volume of distribution at

steady state was similar between 20-nm and 40-nm AuNPs but significantly larger in 80-nm AuNPs (Table 2).

A large body of literature, primarily with liposomal systems, has documented the effect of particle size on the pharmacokinetic behaviors of nanoparticles. These research revealed that the optimal mean diameter for achieving prolonged blood circulation for liposomes is approximately 100 nm [27,28]. It has been suggested that liposomes with diameters < 50 nm are smaller than the pores of live fenestrate and could easily penetrate the endothelial wall, resulting in enhanced liposome uptake in the liver. In polymeric nanoparticles, Fang et al. [29] observed a significant correlation between the particle size and blood clearance of pegylated cyanoacrylate-co-n-hexadecyl cyanoacrylate. In their study, 80-nm nanoparticles were cleared from the blood more than 4 times slower as 243-nm nanoparticles did; however, it was not clear whether particles < 80 nm would have higher liver uptake as had been observed with liposomes due to penetration of the liver fenestration [27,28]. Up to date, a size-dependent pharmacokinetics for nanoparticles with average diameter less than 100 nm has not been systematically studied. In the current study, we found that the 20-nm and 40-nm AuNPs were cleared from the blood more slowly and had less uptake in the liver and spleen than 80-nm AuNPs (see below), suggesting that AuNP uptake in the liver as a result of fenestration penetration is not a dominant factor at sizes as small as 20 nm. Pegylated 20- and 40-nm AuNPs had a higher PEG density than did 80-nm AuNPs. The observed slower blood clearance of smaller AuNPS as compared to larger AuNPS could have been due to higher surface PEG density achievable with smaller AuNPs. The thick PEG layer in 20- and 40-nm AuNPS effectively insulated AuNPs from nonspecific binding to plasma proteins, resulting in reduced liver uptake.

3.5 Biodistribution of PEG-coated AuNPs

Figure 6 shows a typical series of anterior whole-body gamma images recorded 10 min, 2 h, 24 h, and 48 h after injection of pegylated 80-nm and 20-nm AuNPs. The 80-nm AuNPs were rapidly taken up by the liver and the spleen, resulting in their rapid clearance from the blood. There was little overall change in the biodistribution of the 80-nm AuNPs up to 48 h; no activity was found in the kidneys, bladder, or intestines, indicating that the AuNPs had not been excreted via the urinary or hepatobiliary systems. On the other hand, the 20-nm AuNPs showed significant blood pool activity and high uptake in the liver and spleen over the entire study period. Radioactivity was detected in the urine at 10 min and 2 h. It is possible that the injections of 20-nm AuNPs contained a small fraction of nanoparticles with diameters < 5 nm, which could be excreted via the urinary system [30]. By 48 h after injection, the accumulation of the 20-nm AuNPs in the tumor was clearly visualized. The localization to tumor could be attributed to the enhanced permeability and retention effect of long-circulating nanoparticles [19].

Figure 7 shows a comparison of the tissue distribution of ^{111}In-labeled 20-nm and 80-nm AuNPs coated with PEG_{5000}-TA in tumor-bearing mice 48 h after injection. Consistent with the biodistribution evaluated with gamma imaging, the radioactivity in mice injected with both 20-nm and 80-nm AuNPs was largely seen in the liver and the spleen. However, the uptake of AuNPs in the liver (30.31 %ID/g vs. 53.16 %ID/g, $p = 0.005$) and spleen (15.15 %ID/g vs. 62.75 %ID/g, $p = 0.01$) was significantly lower in mice injected with 20-nm AuNPs than in mice injected with 80-nm AuNPs. The 20-nm AuNPs had significantly higher uptake in the heart (1.32 %ID/g vs. 0.15 %ID/g, $p = 0.0001$), indicating their prolonged blood pool activity. The 20-nm AuNPs also had significantly higher activity in the kidneys (4.57 %ID/g vs. 1.14 %ID/g; $p = 0.005$) and intestines (3.63 %ID/g vs. 0.24 %ID/g, $p = 0.001$), suggesting that the smaller AuNPs were more readily excreted via the urinary and hepatobiliary systems. Finally, the 20-nm AuNPs displayed significantly higher tumor uptake (6.63 %ID/g vs. 0.30 %ID/g; $p = 0.0007$). Tumor uptake of PEG_{5000}-TA-coated AuNPs could have been a result of the

AuNPs' prolonged resident time in the blood and their ability to extravasate from tumor blood vessels.

3.6. AuNPs distribution in tumor

To further investigate whether the accumulation of PEG_{5000}-TA-coated 20-nm AuNPs in A431 tumors could be attributed to extravasation of these nanoparticles from the tumor blood vessels, we evaluated the intratumoral distribution of 20-nm AuNPs in A431 tumors. Slices of tumor specimen were immunohistochemically stained for EGFR. Fluorescence microscopic imaging clearly showed that some 20-nm AuNPs had extravasated out of tumor blood vessels 48 h after injection and were mostly distributed in the perivascular area. Some AuNPs in the form of aggregates were also observed in the vessels, suggesting that some particles remained in the blood circulation even at 48 h after injection (Fig. 8). These results confirm that passive targeting to A431 tumors after intravenous injection of 20-nm AuNPS resulted from enhanced permeability and retention effect of nanoparticles.

4. Conclusion

Our findings indicate that PEG layer density via TA ligand depends on AuNP curvature; that is, the smaller the AuNP, the denser its PEG layer. We found that AuNPs coated with PEG_{5000}-TA had the highest colloidal stability, as they did not form aggregates in PBS containing 10 mM DTT or 10% FBS as readily as AuNPs coated with PEG-SH. Through our studies of ^{1111}In-labeled AuNPs coated with PEG_{5000}-TA, we found that AuNPs' pharmacokinetics and biodistribution depend strongly on the size of the nanoparticles; such dependence may be attributed to the dense PEG coating achievable with smaller AuNPs. While 20-nm AuNPs demonstrated prolonged blood circulation and reduced uptake by the liver and the spleen, most 80-nm AuNPs were rapidly taken up by cells of the reticuloendothelial system. The 20-nm AuNPs also appeared to be excreted from the body, which argues for the use of AuNPs < 20 nm in diameter for *in vivo* applications. Significant tumor uptake of 20-nm AuNPs was likely a result of enhanced permeability and retention effect owing to their prolonged blood circulating time and the ability to extravasate from tumor blood vessels. Thus, 20-nm AuNPs coated with TA-terminated PEG_{5000} are promising potential drug delivery vehicles and diagnostic imaging agents.

Acknowledgments

We acknowledge support of National Cancer Institute Grant R01 CA119387 and the John S. Dunn Foundation. We also thank Joe Munch from M. D. Anderson's Department of Scientific Publications for editing the manuscript. The animal studies were performed at the Small Animal Imaging Facility at M. D. Anderson Cancer Center through NCI Grant U24 CA126577.

References

1. Jain PK, Huang X, El-Sayed IH, El-Sayed MA. Noble metals on the nanoscale: optical and photothermal properties and some applications in imaging, sensing, biology, and medicine. Acc Chem Res. 2008 May 1;Epub ahead of print
2. Daniel MC, Astruc D. Gold nanoparticles: assembly, supramolecular chemistry, quantum-size-related properties, and applications toward biology, catalysis, and nanotechnology. Chem Rev 2004;104:293–346. [PubMed: 14719978]
3. Melancon MP, Lu W, Yang Z, Zhang R, Cheng Z, Elliot AM, et al. In vitro and in vivo targeting of hollow gold nanoshells directed at epidermal growth factor receptor for photothermal ablation therapy. Mol Cancer Ther 2008;7:1730–9. [PubMed: 18566244]
4. Zhang F, Skoda MW, Jacobs RM, Zorn S, Martin RA, Martin CM, et al. Gold nanoparticles decorated with oligo(ethylene glycol) thiols: protein resistance and colloidal stability. The journal of physical chemistry 2007;111:12229–37. [PubMed: 17914772]

5. Otsuka H, Nagasaki Y, Kataoka K. PEGylated nanoparticles for biological and pharmaceutical applications. Advanced drug delivery reviews 2003;55:403–19. [PubMed: 12628324]
6. Paciotti GF, Myer L, Weinreich D, Goia D, Pavel N, McLaughlin RE, et al. Colloidal gold: a novel nanoparticle vector for tumor directed drug delivery. Drug Deliv 2004;11:169–83. [PubMed: 15204636]
7. Hainfeld JF, Slatkin DN, Focella TM, Smilowitz HM. Gold nanoparticles: a new X-ray contrast agent. Br J Radiol 2006;79:248–53. [PubMed: 16498039]
8. Kim D, Park S, Lee JH, Jeong YY, Jon S. Antibiofouling polymer-coated gold nanoparticles as a contrast agent for in vivo X-ray computed tomography imaging. J Am Chem Soc 2007;129:7661–5. [PubMed: 17530850]
9. Qian X, Peng XH, Ansari DO, Yin-Goen Q, Chen GZ, Shin DM, et al. In vivo tumor targeting and spectroscopic detection with surface-enhanced Raman nanoparticle tags. Nat Biotechnol 2008;26:83–90. [PubMed: 18157119]
10. Takae S, Akiyama Y, Otsuka H, Nakamura T, Nagasaki Y, Kataoka K. Ligand density effect on biorecognition by PEGylated gold nanoparticles: regulated interaction of RCA120 lectin with lactose installed to the distal end of tethered PEG strands on gold surface. Biomacromol 2005;6:818–24.
11. De Jong WH, Hagens WI, Krystek P, Burger MC, Sips AJ, Geertsma RE. Particle size-dependent organ distribution of gold nanoparticles after intravenous administration. Biomaterials 2008;29:1912–9. [PubMed: 18242692]
12. James WD, Hirsche LR, West JL, O'Neal PD, Payne JD. Application of INAA to the build-up and clearance of gold nanoshells in clinical studies in mice. J Radioanal Nucl Chem 2007;271:455–9.
13. Niidome T, Yamagata M, Okamoto Y, Akiyama Y, Takahashi H, Kawano T, et al. PEG-modified gold nanorods with a stealth character for in vivo applications. J Control Release 2006;114:343–7. [PubMed: 16876898]
14. Foos EE, Snow AW, Twigg ME, Ancona MG. Thiol-terminated di-, tri-, and tetraethylene oxide functionalized gold nanoparticles: a water-soluble, charge-neutral cluster. Chem Mater 2002;14:2401–8.
15. Tshikhudo TR, Wang Z, Brust M. Biocompatible gold nanoparticles. Mat Sci & Technol 2004;20:980–4.
16. Dougan JA, Karlsson C, Smith WE, Graham D. Enhanced oligonucleotide-nanoparticle conjugate stability using thioctic acid modified oligonucleotides. Nucleic Acids Res 2007;35:3668–75. [PubMed: 17488844]
17. Li Z, Jin R, Mirkin CA, Letsinger RL. Multiple thiol-anchor capped DNA-gold nanoparticle conjugates. Nucleic Acids Res 2002;30:1558–62. [PubMed: 11917016]
18. Dixit V, Van den Bossche J, Sherman DM, Thompson DH, Andres RP. Synthesis and grafting of thioctic acid-PEG-folate conjugates onto Au nanoparticles for selective targeting of folate receptor-positive tumor cells. Bioconjug Chem 2006;17:603–9. [PubMed: 16704197]
19. Yang Z, Zheng S, Harrison WJ, Harder J, Wen X, Gelovani JG, et al. Long-circulating near-infrared fluorescence core-cross-linked polymeric micelles: synthesis, characterization, and dual nuclear/optical imaging. Biomacromol 2007;8:3422–8.
20. Weissig V, Whiteman KR, Torchilin VP. Accumulation of protein-loaded long-circulating micelles and liposomes in subcutaneous Lewis lung carcinoma in mice. Pharm Res 1998;15:1552–6. [PubMed: 9794497]
21. Kommareddy S, Amiji M. Biodistribution and pharmacokinetic analysis of long-circulating thiolated gelatin nanoparticles following systemic administration in breast cancer-bearing mice. J Pharm Sci 2007;96:397–407. [PubMed: 17075865]
22. Singh R, Pantarotto D, Lacerda L, Pastorin G, Klumpp C, Prato M, et al. Tissue biodistribution and blood clearance rates of intravenously administered carbon nanotube radiotracers. Proc Natl Acad Sci U S A 2006;103:3357–62. [PubMed: 16492781]
23. Zhang G, Zhang R, Wen X, Li L, Li C. Micelles based on biodegradable poly(L-glutamic acid)-b-polylactide with paramagnetic Gd ions chelated to the shell layer as a potential nanoscale MRI-visible delivery system. Biomacromol 2008;9:36–42.
24. Hurst SJ, Lytton-Jean AK, Mirkin CA. Maximizing DNA loading on a range of gold nanoparticle sizes. Anal Chem 2006;78:8313–8. [PubMed: 17165821]

25. Tanford C, Nozaki Y, Rohde MF. Size and shape of globular micelles formed in aqueous-solution by normal-alkyl polyoxyethylene ethers. J Phys Chem 1977;81(16):1555–60.

26. Liu Y, Shipton MK, Ryan J, Kaufman ED, Franzen S, Feldheim DL. Synthesis, stability, and cellular internalization of gold nanoparticles containing mixed peptide-poly(ethylene glycol) monolayers. Anal Chem 2007;79:2221–9. [PubMed: 17288407]

27. Li SD, Huang L. Pharmacokinetics and biodistribution of nanoparticles. Mol Pharm 2008;5:496–504. [PubMed: 18611037]

28. Liu D, Mori A, Huang L. Role of liposome size and RES blockade in controlling biodistribution and tumor uptake of GM1-containing liposomes. Biochim Biophys Acta 1992;1104:95–101. [PubMed: 1550858]

29. Fang C, Shi B, Pei YY, Hong MH, Wu J, Chen HZ. In vivo tumor targeting of tumor necrosis factor-alpha-loaded stealth nanoparticles: effect of MePEG molecular weight and particle size. Eur J Pharm Sci 2006;27:27–36. [PubMed: 16150582]

30. Choi HS, Liu W, Misra P, Tanaka E, Zimmer JP, Itty Ipe B, et al. Renal clearance of quantum dots. Nat Biotechnol 2007;25:1165–70. [PubMed: 17891134]

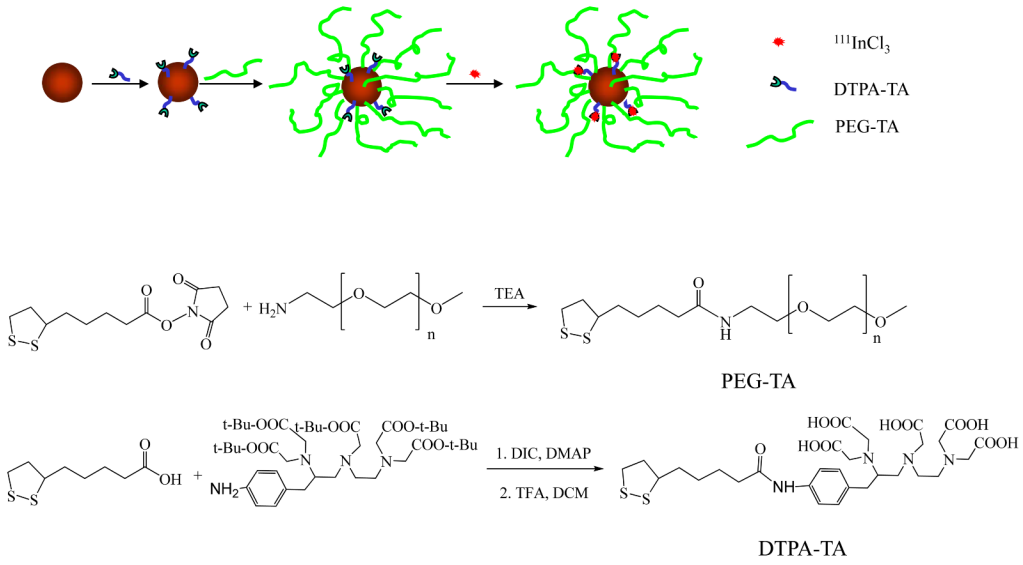

Fig. 1.

(A) Schematic of the synthesis of indium-111 (^{111}In)-labeled, polyethylene glycol (PEG)-coated gold nanoparticles using thioctic acid (TA) as an anchoring ligand. (B) Synthesis of PEG-TA. (C) Synthesis of 4-aminobenzyl-diethylenetriaminepentaacetic acid thioctamide (DTPA-TA). TEA, triethylamine; DIC, 1,3-diisopropylcarbodiimide; DMAP, 4-dimethylaminopyridine; TFA, trifluoroacetic acid; DCM, dichloromethane.

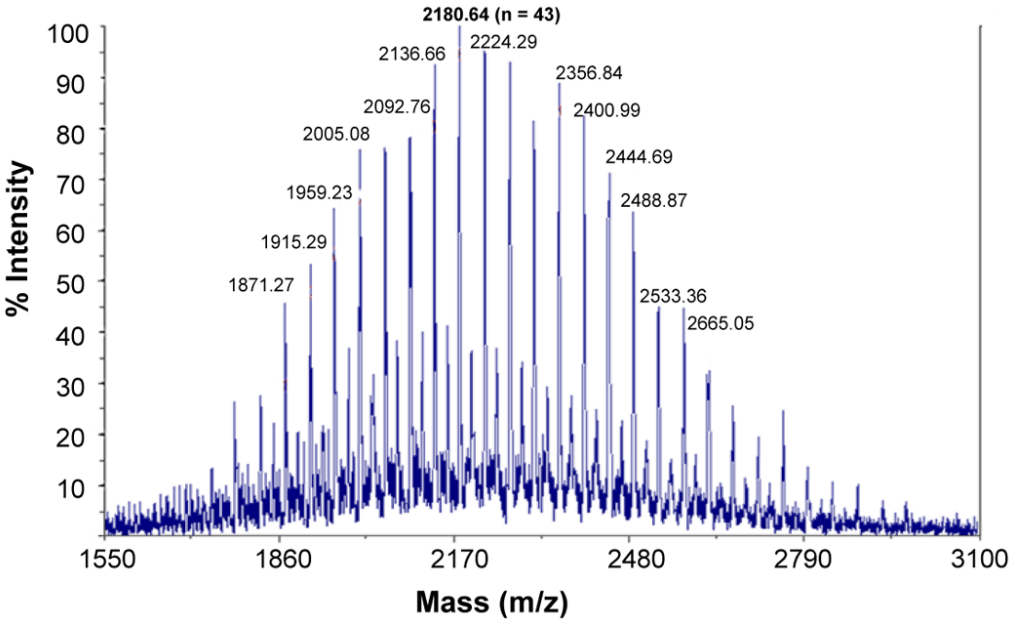

Fig. 2.

Matrix-assisted laser desorption/ionization time-of-flight mass spectrum of O-(2-aminoethyl)-O′-methyl polyethylene glycol (molecular weight, 2000) terminated with thioctic acid (TA). The polydispersity index was 1.02. The intensity peak at 2180.64 corresponded to MeO-$(CH_2CH_2O)_{43}$-TA/Na^+.

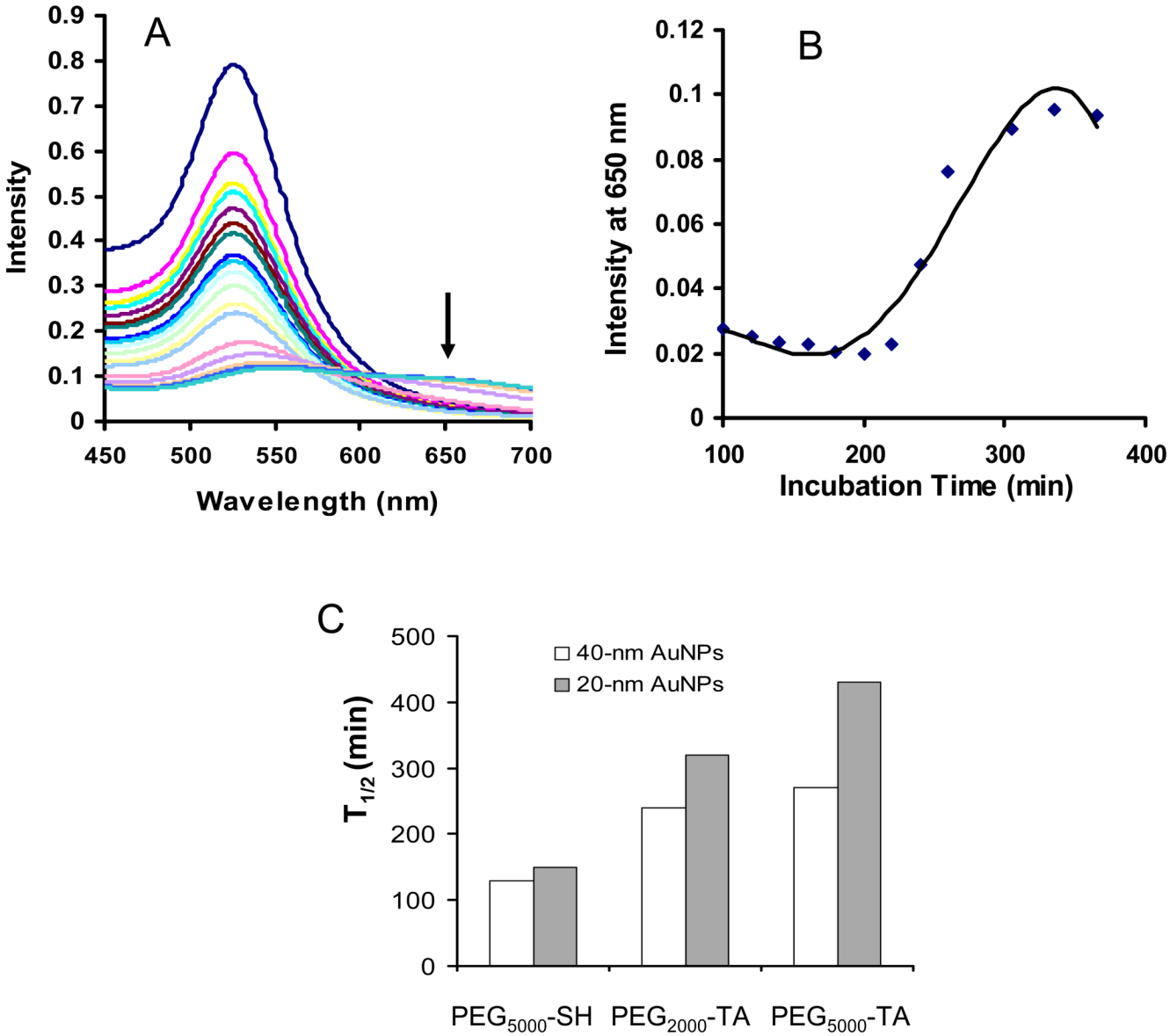

Fig. 3.

Stability of pegylated gold nanoparticles (AuNPs) in phosphate-buffered saline containing 10 mM dithiothreitol (DTT) at 40°C. (A) Ultraviolet-visible spectra of 40- nm AuNPs coated with thiol-terminated polyethylene glycol with a molecular weight of 5000 (PEG_{5000}-SH) acquired at various times after the addition of DTT. The concentration of AuNPs was 7.0×10^{11} particles/ml. The arrow in the figure denotes absorbance at 650 nm. (B) Absorbance at 650 nm as a function of time. (C) Half-lives for 20-nm and 40-nm AuNPs coated with different types of PEG.

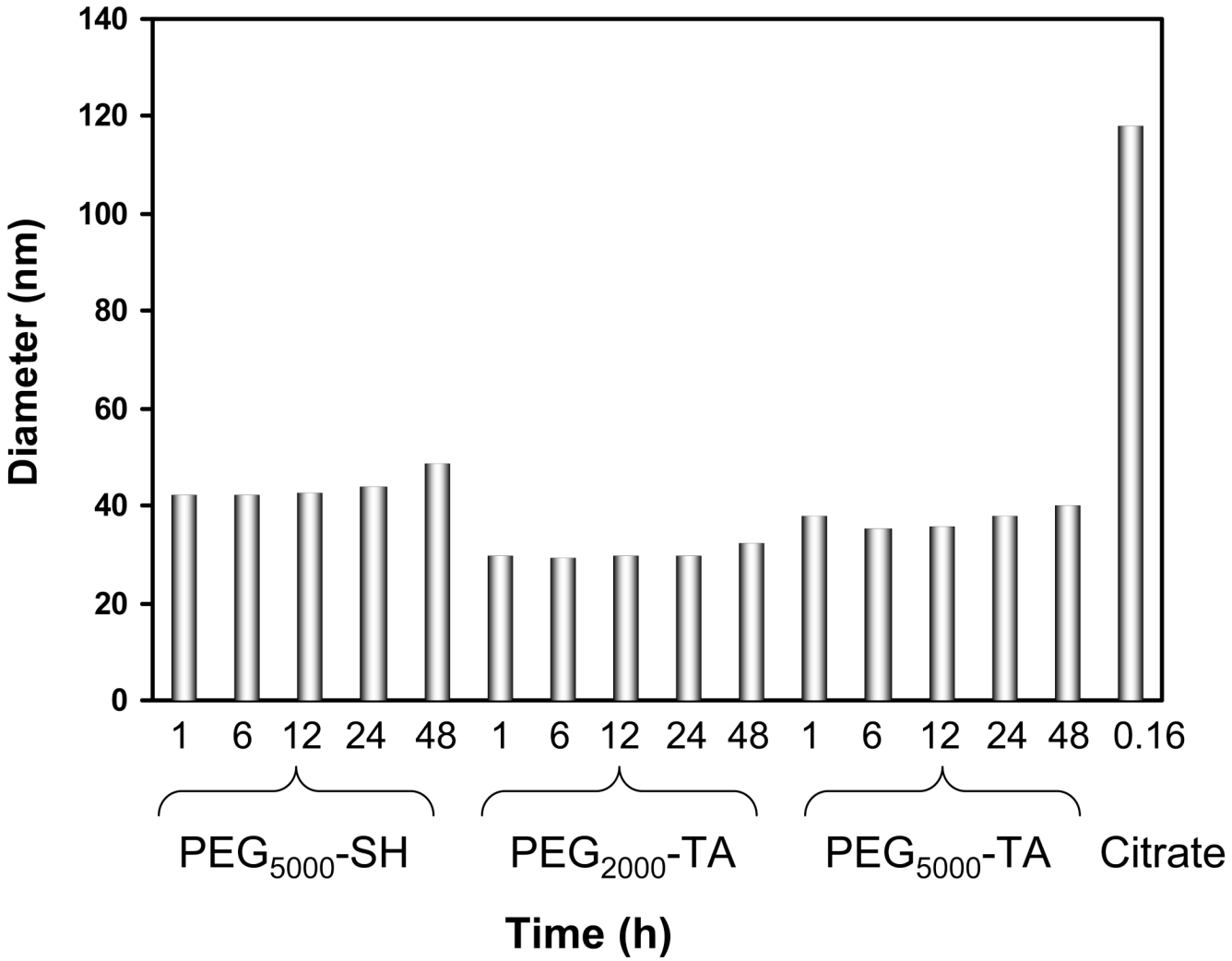

Fig. 4.

Stability of 20-nm gold nanoparticles (AuNPs) in phosphate-buffered saline containing 10% fetal bovine serum at 37°C. The diameters of nanoparticles were measured using dynamic light scattering. Pegylated AuNPs did not show a significant change in particle size, whereas plain (uncoated) AuNPs aggregated within 10 min after incubation.

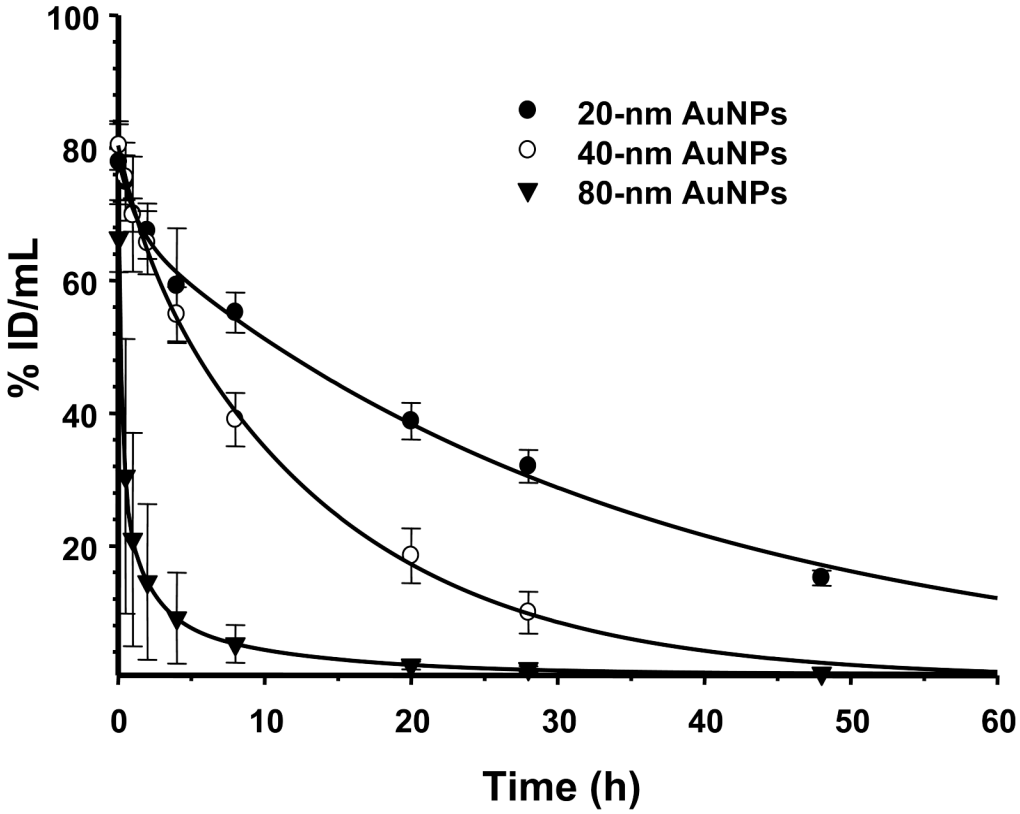

Fig. 5.
Pharmacokinetics, expressed as the percentage of the injected dose per gram of tissue in mice (%ID/g), of 20-nm, 40-nm, and 80-nm gold nanoparticles (AuNPs) coated with thioctic acid-terminated polyethylene glycol. The solid lines are curves fitted to a two-compartment model.

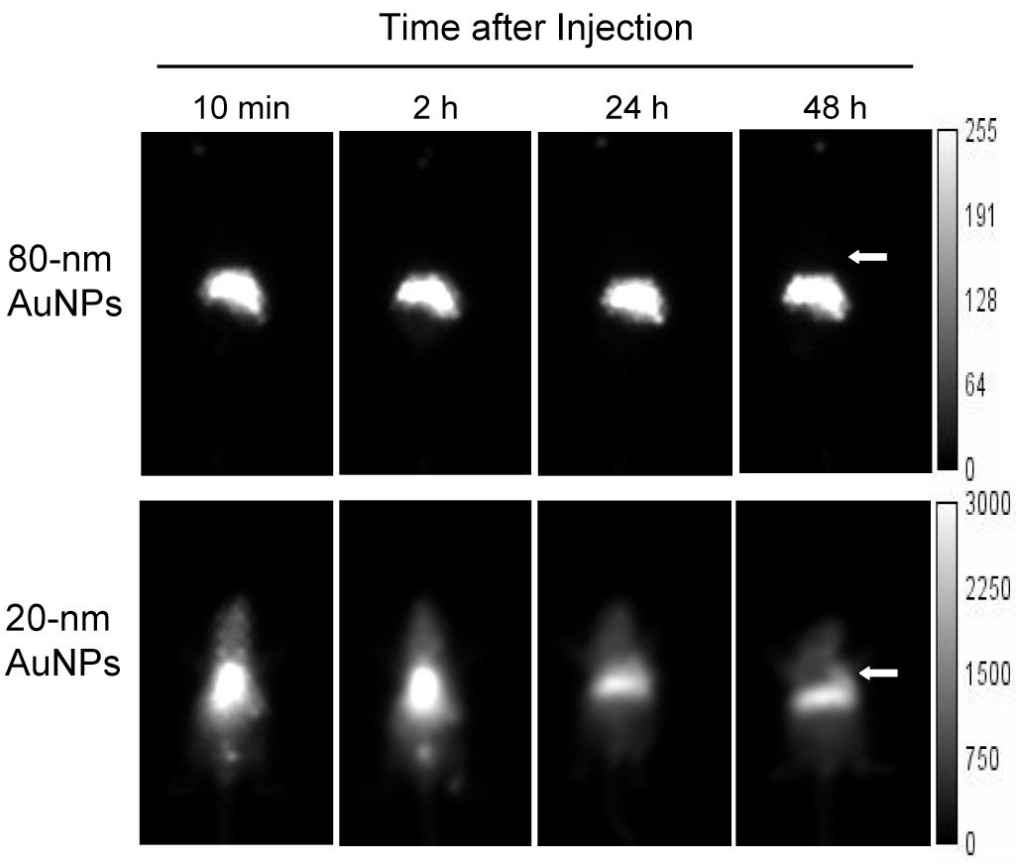

Fig. 6.

Gamma images of the *in vivo* distribution of 80-nm and 20-nm gold nanoparticles (AuNPs) in mice bearing A431 tumors 10 min and 2, 24, and 48 h after intravenous injection. Compared to 20-nm AuNPs, 80-nm AuNPs were cleared more rapidly from the blood and had higher concentrations in the liver and spleen. In contrast, 20-nm AuNPs had long blood pool activity and accumulated in the tumor 48 h after injection. The scales on the right side of each panel show the signal intensity range. Arrows indicate subcutaneous A431 tumors.

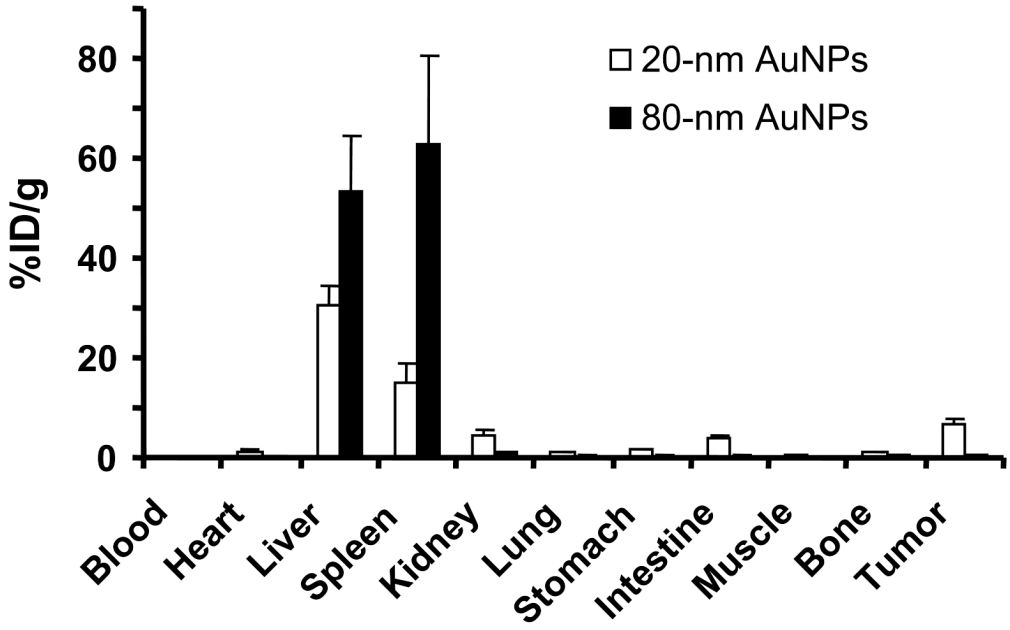

Fig. 7.

Biodistribution of 20-nm and 80-nm gold nanoparticles (AuNPs) coated with thioctic acid-anchored polyethylene glycol with a molecular weight of 5000 in mice bearing subcutaneous A431 tumors.

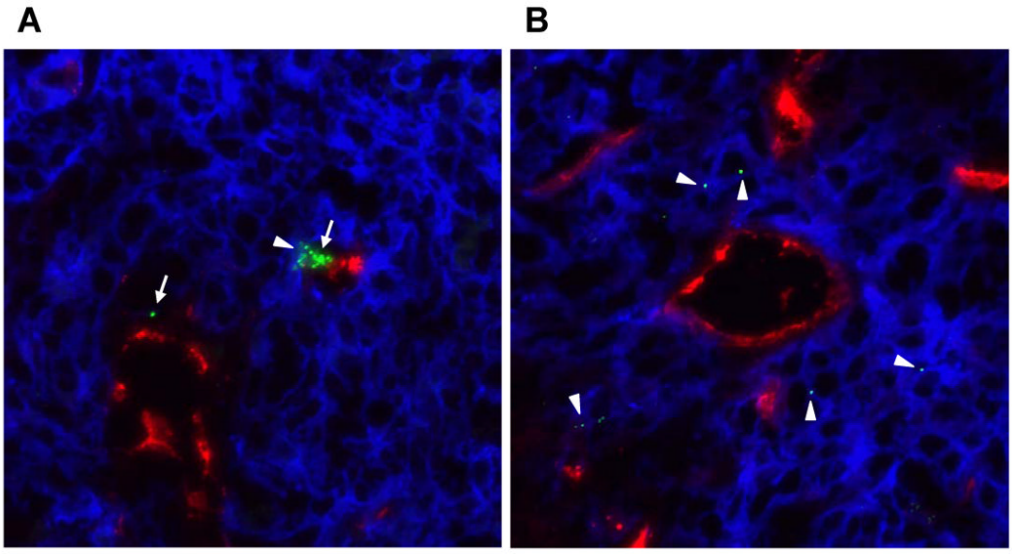

Fig. 8.

Fluorescence microscopic image (original magnification, 40×) of a 5-μm cryosectioned slice of an A431 tumor removed from a mouse 48 h after intravenous injection of 20-nm gold nanoparticles (AuNPs) coated with thioctic acid-anchored polyethylene glycol with a molecular weight of 5000. The slice was stained for platelet-endothelial cell adhesion molecule-1 (CD31, red) and epidermal growth factor receptor (blue). AuNPs were visualized using a dark field condenser (pseudocolored green). (A) Some nanoparticles remained in the blood vessel (arrows), while (B) others entered the extravascular fluid space (arrow heads).

Table 1

Physicochemical properties of plain and polyethylene glycol (PEG)-coated gold nanoparticles (AuNPs)

Nanoparticle	Surface coating			
	Citrate	PEG_{2000}-TA	PEG_{5000}-TA	PEG_{5000}-SH
20-nm AuNPs				
Size, nm (polydispersity)	20.0	36.3 (0.086)	45.4 (0.093)	47.6 (0.091)
ζ potential, mV	−38.0	−8.6	−7.4	−8.1
PEG thickness, nm	--	8.2	12.7	13.8
40-nm AuNPs				
Size, nm (polydispersity)	40.0	50.3 (0.119)	60.0 (0.086)	59.2 (0.130)
ζ potential, mV	−34.0	−8.7	−7.4	−8.1
PEG thickness, nm	--	5.0	9.8	9.6
80-nm AuNPs				
Size, nm (polydispersity)	80.0	82.3 (0.167)	89.3 (0.159)	86.6 (0.146)
ζ potential, mV	−41.0	−11.1	−9.4	−8.7
PEG thickness, nm	--	1.2	4.7	3.3

Abbreviations: PEG_{2000}-TA, thioctic acid-anchored PEG with a molecular weight of 2000; PEG_{5000}-TA, thioctic acid-anchored PEG with a molecular weight of 5000; PEG_{5000}-SH, thiol-anchored PEG with a molecular weight of 5000.

Table 2

Plasma pharmacokinetics of gold nanoparticles (AuNPs) coated with thioctic acid-anchored polyethylene glycol with a 5000-Da molecular weight after intravenous injection.

AuNP size	$t_{1/2\alpha}$ (h)	$t_{1/2\beta}$ (h)	AUC (%ID h/ml)	V_d(ss) (ml)	CL (ml/h)	MRT (h)
20 nm	0.49±0.31	22.5±1.1	2273.4±159.7	1.43±0.14	0.044±0.030	32.4±1.5
40 nm	1.32±0.60	10.1±1.6**	1039.2±177.7**	1.38±0.04	0.098±0.017**	14.3±2.3**
80 nm	0.80±0.89	15.8±2.7**	192.2±86.6**	9.68±3.84*	0.590±0.220*	16.0±1.9**

Values are means ± standard deviations calculated for 8 mice from each group after intravenous injection.

Abbreviations: $t_{1/2\alpha}$, blood half-life distribution; $t_{1/2\beta}$, blood half-life clearance; AUC, area under the curve for blood activity-time curve; Vd(ss), volume of distribution at steady-state; CL, total body clearance; MRT, mean residence time.

* $p < 0.05$;

** $p < 0.01$ compared with the corresponding parameters of the 20-nm AuNPs formulation.